Ferroelastic domain freezing and low-frequency elastic behaviour of $(NH_4)_4LiH_3(SO_4)_4$ (ALHS)

1996 J. Phys.: Condens. Matter 8 7085

(http://iopscience.iop.org/0953-8984/8/38/013)

J. Phys.: Condens. Matter **8** (1996) 7085–7103. Printed in the UK

Ferroelastic domain freezing and low-frequency elastic behaviour of $(NH_4)_4LiH_3(SO_4)_4$ (ALHS)

M Zimmermann and W Schranz

Institute of Experimental Physics, University of Vienna, Strudlhofgasse 4, A-1090 Vienna, Austria

Received 5 February 1996

Abstract. In this work elastic measurements on $(NH_4)_4LiH_3(SO_4)_4$ (ALHS) which were carried out in the low-frequency range between 1 and 50 Hz are presented. The temperature dependence of the inverse elastic compliance S_{11}^{-1} has been determined between 90 K and 420 K. Distinct anomalies have been found in the temperature dependence of S_{11}^{-1}, which are connected to the motion of domain walls in the ferroelastic phase below $T_c = 232.5$ K. Around $T_f = 162$ K a (partial) ferroelastic 'domain freezing' phenomenon has been observed. To the knowledge of the authors this is the first time that pure ferroelastic domain freezing has been reported. However, below T_f the domain walls seem to retain a certain vibrational degree of freedom which could be responsible for an additional anomaly of the loss modulus which was observed.

The elastic behaviour of a crystal of ALHS is dependent on the 'history' of the given sample. During temperature cycling S_{11}^{-1} shows differences between the first run of heating and cooling and later runs.

Finally, some basic insights concerning the domain wall motion were obtained; it was found that the domain wall mobility decreases by three orders of magnitude in the temperature region 170–230 K.

1. Introduction

$(NH_4)_4LiH_3(SO_4)_4$, abbreviated as ALHS, belongs to the family of ferroelastic crystals $M_4LiZ_3(XO_4)_4$ ($M = K, Rb, NH_4$; $Z = H, D$; $X = S, Se$). At room temperature it is tetragonal with space group $P4_1$. Below the phase transition at $T_c = 233$ K the ferroelastic phase is monoclinic with space group $P2_1$ [1, 2]. Optical studies confirmed the second-order type of this phase transition [3] which is a proper one with spontaneous strain as the primary order parameter [4].

The elastic instabilities occur in the plane perpendicular to the tetragonal axis (the c-axis); for the soft elastic constant complete softening was found [5]. Elastic studies of ALHS below room temperature were performed by Brillouin scattering [5], by piezoelectric investigations [6], and by torsional vibration and static dilatometry [4].

For the room temperature lattice constants of ALHS, $a = 7.642$ Å and $c = 29.566$ Å have been found [1]. Recently 'superionic' behaviour of ALHS was reported [7, 8]. The transition temperature T_s of the associated 'protonic' transition [9] was found to be around 415 K. At about 430 K melting of the crystal occurs [8].

The ferroelastic domain walls form angles of 33° and 57° with respect to the tetragonal crystallographic axes [3, 10]. It is interesting to notice that 33° is about the angle of the

0953-8984/96/387085+19$19.50

hypotenuse of a rectangular triangle with a cathetus ratio of 2:3. Besides this, the line connecting the sulphur atoms S2 and S3 in the unit cell of ALHS† has about this angle.

An ND_4 deuteron NMR study of the ferroelastic phase and the phase transition of the closely related substance $(ND_4)_4LiD_3(SO_4)_4$ is presented in [11]. Additionally, ^1H [12] and ^{14}N [13] NMR investigations of ALHS have already shown that H bonds and NH_4 groups are not connected to the elastic anomalies found in the ferroelastic phase. These elastic anomalies were observed in the low-frequency range between 1 and 50 Hz using a Dynamic Mechanical Analyzer (DMA). The measured temperature dependence of the inverse elastic compliance S_{11}^{-1} (effective elastic constant) shows similarities to the temperature dependence of the elastic constant C_{66} in KD_2AsO_4 [14]. As the elastic and dielectric anomalies in that crystal (which is ferroelectric and ferroelastic at the same time) are caused by 'domain freezing' this suggested investigating whether something equivalent happens also in ALHS which is only ferroelastic. 'Domain freezing' can be observed if the relaxation time which is related to the motion of domain walls diverges at a certain temperature (the 'freezing temperature'). Often such a 'freezing' of domain wall motion (or 'pinning' of domain walls) is caused by defects in the crystal structure. In order to find out whether ALHS actually exhibits pure ferroelastic domain freezing (which according to the author's knowledge has not ever been reported before), various measurements of the dependence of various quantities (temperature, frequency, direction) have been performed. The results of these studies are presented and interpreted in this work.

2. Experimental procedures and results

2.1. Samples and their preparation

Crystals of ALHS were grown at room temperature from a non-stoichiometric acid aqueous solution of Li_2SO_4, $(NH_4)_2SO_4$, and H_2SO_4 by slow evaporation of water. They were hygroscopic and appeared in the form of rectangular plates or truncated pyramids with a typical side length of $\cong$5 mm. The plates were found to be oriented perpendicular to the [001] direction. Their sides were parallel to the remaining tetragonal crystal axes. The orientation of all the plates used for DMA measurements was checked by conoscopical observation with a polarizing microscope. In order to check the composition and structure of the samples, x-ray powder diffraction was performed at room temperature [9], the results of which could be well described by the lattice parameters already published in the literature.

The samples were cut and polished; during sample preparation it was found out that stress imposed on the sample during cutting does not influence the ferroelastic domain pattern. In addition, the domain wall orientations do not change during several consecutive runs of temperature cycling.

In order to be able to detect whether there are effects stemming from single-crystal plates or from defects, the samples used for the experiments were cut from different crystal plates grown in different vessels which were filled with solutions prepared at different times from different chemical sources.

2.2. Experimental methods

The static and low-frequency elastic properties of ALHS were investigated with a Perkin–Elmer Dynamic Mechanical Analyzer (DMA 7). Within this apparatus the samples are exposed to a given static force which is modulated by a dynamic force of chosen amplitude

† Structural data obtained from A Pietraszko, Wrocław, 1994.

and frequency. The amplitude u and the phase shift δ of the resulting elastic response of a sample are registered via inductive coupling with a resolution of $\Delta u \cong 10$ nm and $\Delta\delta \cong 0.1^\circ$. The knowledge of δ and u allows the determination of the real and the imaginary parts of the inverse elastic compliance, storage and loss modulus, $C^{eff} = S^{-1}$ (see pp 38–40 of [15] and pp 2–4 of [16]):

$$C^{eff\prime} = C^{eff}\cos\delta \qquad \text{and} \qquad C^{eff\prime\prime} = C^{eff}\sin\delta. \tag{1}$$

The force is transmitted by a quartz rod, which is also the probe for the position of the upper end of the sample. The sample itself is placed within a sample holder made of quartz, too. The displacement sensitivity is 0.2 μm (sample dimensions perpendicular to the direction of measurement were determined with an accuracy of 10 μm).

Applied forces were chosen high enough to guarantee elastic amplitude values distinctly larger than the above-mentioned resolution of Δu (i.e., in the region of μm). Hence the error of the measured (relative) values of C^{eff} is in the region of some per cent.

The minimum temperature available during DMA experiments was ~90 K; the temperature values are obtained with a resolution of 0.1 K. The available frequencies were 1–50 Hz; because of the low frequencies (quasistatic measurements) the elastic compliance is proportional to the elastic amplitude (see below).

Typical sample dimensions were in the region of a few mm; samples exposed to three-point bending had a thickness of some tenths of a mm. The estimated uncertainty of the stress values is ±10%, resulting from irregularities in the shapes of the samples and from errors of the thickness measurements. Thus the determination of relative changes is more precise than that of absolute values of C^{eff}.

In a parallel-plate measurement a sample is exposed to a force F acting on the whole cross section A (which is perpendicular to the long side L of the sample). This produces a homogeneous stress profile within the sample leading to an elastic deformation amplitude u. Then the elastic compliance is given (see pp 37, 38 of [15] and pp 660–3 of [17]) by

$$S^{eff} = \frac{uA}{LF}. \tag{2}$$

During most of the experiments the parallel-plate technique was used.

For the investigation of the direction dependence of the domain wall contribution to the measured elastic compliance it was necessary to prepare samples whose sides formed an angle of 33° with the crystallographic a-axis. Because it proved to be easier to prepare such samples for three-point bending, this mode of the DMA apparatus was applied in this case.

A dynamic force P is applied on a sample resting on two edges. The resulting bending moment creates an inhomogeneous stress profile within the sample. S^{eff}, the measured elastic compliance, is then proportional to the amplitude (see p 34 of [15] and p 666 of [17]):

$$S^{eff} \approx \frac{4H^3Du}{PL^3}. \tag{3}$$

H and D are the height and depth of the sample, while L is the distance of the edges of the three-point-bending apparatus.

2.3. Experimental results

2.3.1. 'History' dependence. The term 'history' was chosen to express the fact that the experimental results obtained were distinctly dependent on the treatment that the sample

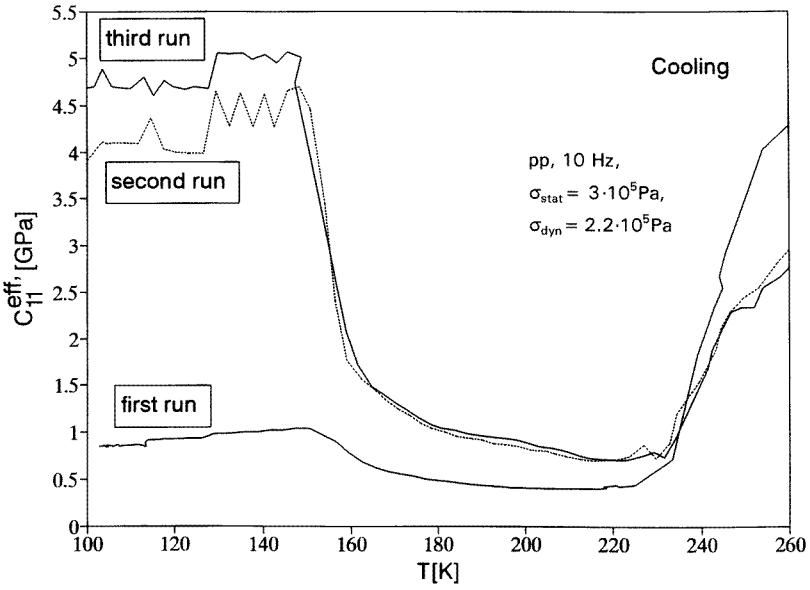

Figure 1. Measured values of $C^{eff\,\prime}$ for several consecutive runs.

was exposed to before the actual measurement. Measurements of C_{11}^{eff} revealed during temperature cycling the behaviour described below (in order to emphasize the characteristics, only lines connecting the measured values are shown in figure 1). The absolute value of $C_{11}^{eff\,\prime}$ was found to be $(6 \pm 0.6) \times 10^9$ Pa at room temperature. This may be compared with the value of $C_{11}^{eff\,\prime}$ (which is equal to $(S'_{11})^{-1}$, because $S''_{11} \approx 0$ at room temperature) calculated from the results given in [5]: 5.9×10^9 Pa. *Hence good agreement is found.*

(1) *The first cooling (see figures 1 and 2).* Starting from room temperature $C_{11}^{eff\,\prime}$ decreases, reaching a minimum at T_c. Then $C_{11}^{eff\,\prime}$ remains rather small, showing only a very small increase with decreasing temperature (comparing Brillouin measurements [5] below T_c one would have expected $C_{11}^{eff\,\prime}$ to rise again significantly). At around 162 K $C_{11}^{eff\,\prime}$ rises to reach a value of about 1 GPa which remains almost constant down to ∼100 K (the lower-temperature limit of the DMA).

$C_{11}^{eff\,\prime\prime}$, which is very near zero in the paraelastic phase, shows a maximum at T_c. Below T_c it remains larger than zero due to the appearance of ferroelastic domains. Sometimes a maximum at around 190 K is observed. At the temperature where $C_{11}^{eff\,\prime}$ shows a step, $C_{11}^{eff\,\prime\prime}$ exhibits a maximum (this maximum is higher than the maximum observed at T_c—compare ferroelectric KDP [18]). In analogy to the results for ferroelectric materials this temperature (of about 162 K) will be denoted by T_f.

Below T_f, $C_{11}^{eff\,\prime\prime}$ decreases, but then unexpectedly rises again to reach another maximum. The height of this 'low-temperature damping maximum' is much larger if the crystal has not been exposed to temperature cycling before or, as it seems here, if it has been annealed at higher temperatures, i.e., ∼400 K (compare figures 2 and 3).

(2) *The first heating (see figure 3).* On heating up again, the behaviour described for cooling is reproduced in the opposite direction. The only difference is that for static stress

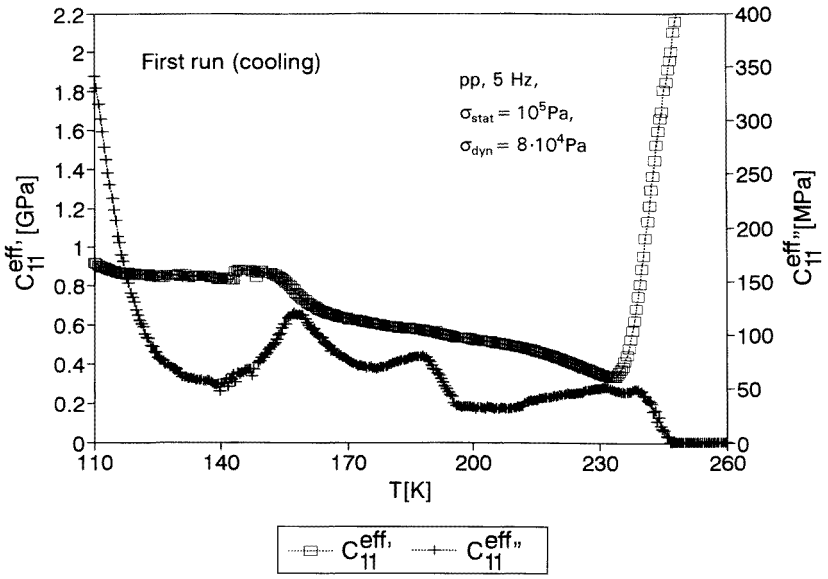

Figure 2. Measured values of the real and imaginary parts of C^{eff}.

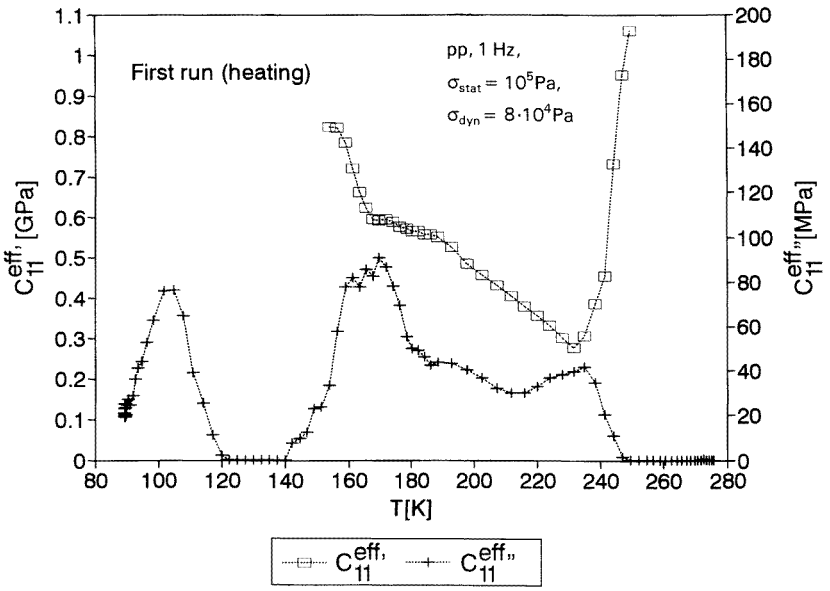

Figure 3. Measured values of the real and imaginary parts of C^{eff}.

values $\geqslant$some 10^5 Pa, $C_{11}^{eff\prime}$ increases slightly below T_c, thus producing a V-shaped minimum at around T_c. $C_{11}^{eff\prime\prime}$ shows the same temperature dependence as for cooling.

(3) *The second cooling (see figure 1).* On cooling down directly (i.e., within some minutes) after the first heating has finished, the following is found. Again $C_{11}^{eff\prime}$ reaches a

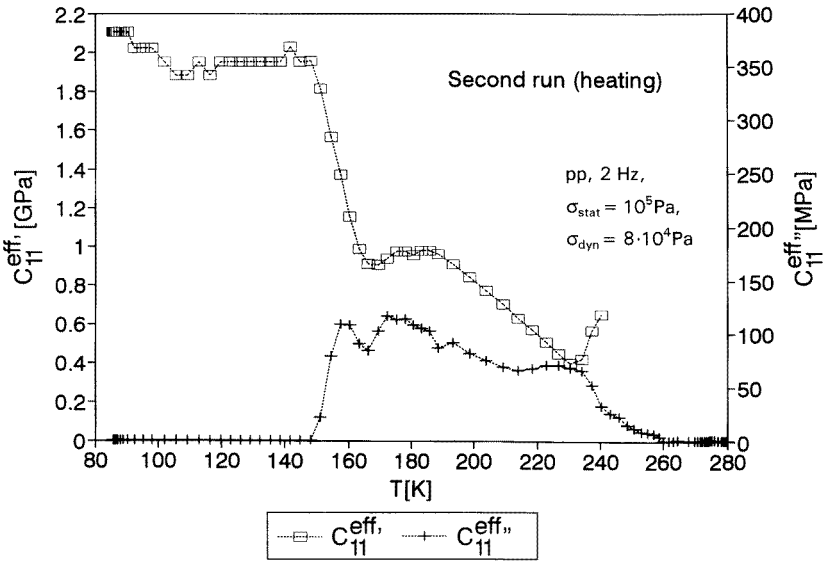

Figure 4. Measured values of the real and imaginary parts of C^{eff}.

minimum at T_c, and remains rather small below T_c (although not as small as during the first run). At T_f, $C_{11}^{eff\prime}$ rises to much higher values than during the first run. Sometimes even the room temperature value of $C_{11}^{eff\prime}$ is reached. The value of $C_{11}^{eff\prime}$ below T_f is not always constant; sometimes it decreases by some GPa. The maximum of $C_{11}^{eff\prime\prime}$ at around T_c is higher with respect to the maximum at around T_f than during the first run. The maximum of $C_{11}^{eff\prime\prime}$ below T_f (the 'low-temperature damping maximum') more or less vanished in all of the later runs.

(4) *The second heating (see figure 4).* On heating again, $C_{11}^{eff\prime}$ decreases at T_f, reaching about the same values as during cooling. Sometimes an additional maximum of $C_{11}^{eff\prime}$ occurs at around 190 K which is accompanied by a maximum in $C_{11}^{eff\prime\prime}$. The features around T_c are similar to those in the first heating. $C_{11}^{eff\prime\prime}$ does not show any new aspects.

(5) *Later runs (see figure 1).* Later runs started directly after the runs before reveal the same behaviour as the second run of consecutive temperature cyclings. Only the values of $C_{11}^{eff\prime}$ are not exactly reproduced below T_f.

The recorded differences might be compared with observations of the domain structure where different patterns were found for first and later runs [9].

After leaving the samples at room temperature for several hours (one night) at zero external stress, the behaviour of a first run could be reproduced.

This did not work at low temperatures—two different experiments were carried out at 100 K. (i) A sample having crossed the phase transition temperature only once was left at zero stress for 8 h: $C_{11}^{eff\prime}$ did not change. (ii) Then a sample having been cooled for the second time during temperature cycling was left at zero stress for 8 h. Also here $C_{11}^{eff\prime}$ did not change.

The temperature dependence of C_{11}^{eff} above room temperature is shown in figure 5: for

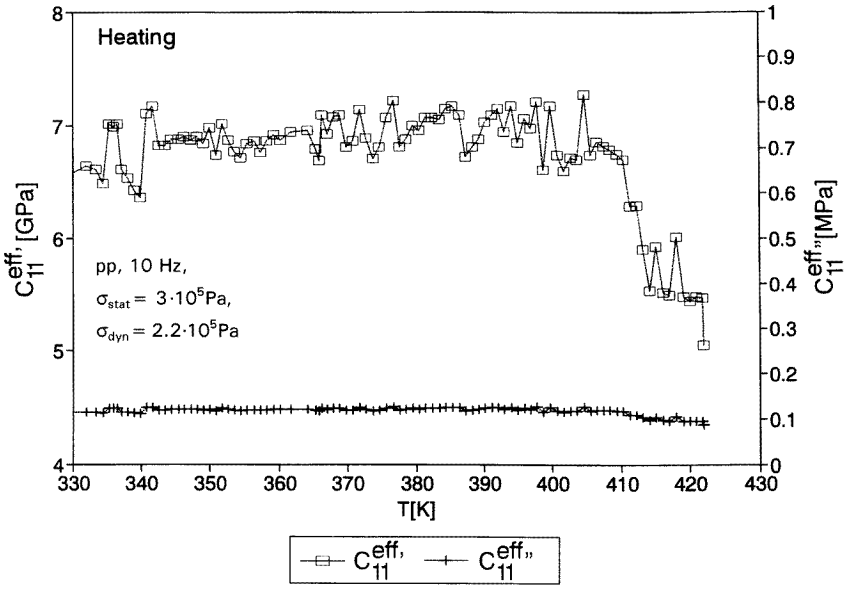

Figure 5. Measured values of C_{11}^{eff} above room temperature.

rising temperature the storage modulus $C_{11}^{eff\prime}$ remains constant. Around 410 K it starts to decrease until the melting point is reached. It is interesting to note that this is *near the temperature where dielectric properties change and ALHS exhibits a 'protonic' transition* ($T_s \approx 415$ K) [8, 9]. The loss modulus $C_{11}^{eff\prime\prime}$ remains very small over the whole temperature range.

2.3.2. Frequency dependence. In the case of ferroelastic domain freezing one would expect a frequency dependence of T_f (see section 4.1). However, no such dependence could be found. Plotting T_f versus frequency no clear dependence could be found. The only clear result obtained was that T_f lies at 162 K $\pm$ some degrees (the uncertainty results from the statistical scattering of the experimental values around 162 K). In section 4.1 we will try to estimate at least some limits of the parameters describing the ferroelastic domain freezing in ALHS.

A clearer picture could be gained from the frequency dependence of the low-temperature damping maximum. Two different fitting attempts have been made: an Arrhenius law (equation (4)) as well as a Vogel–Fulcher law (equation (5)) [19] have been taken as fitting functions:

$$(\tau_2^{rel})_A = \tau_2^0 \exp\left(\frac{E_2^{act}}{T}\right) \tag{4}$$

$$(\tau_2^{rel})_{VF} = \tau_2^0 \exp\left(\frac{E_2^{act}}{T - T_{VF}}\right) \tag{5}$$

where E_2^{act} is the activation energy related to the process considered and T_{VF} is the Vogel–Fulcher temperature.

Fitting with a Vogel–Fulcher law one obtains

$$E_2^{act} \cong 0.0036 \pm 0.0040 \text{ eV } (42 \text{ K}) \qquad T_{VF} \cong 85.5 \pm 8.3 \text{ K}$$
$$\tau_2^0 \cong 1.7 \times 10^{-3} \text{ s} \qquad (\ln(\tau_2^0) = -6.43 \pm 1.34).$$

The fit according to an Arrhenius law yields

$$E_2^{act} \cong 0.119 \pm 0.024 \text{ eV } (1379 \text{ K})$$
$$\tau_2^0 \cong 3.7 \times 10^{-8} \text{ s} \qquad (\ln(\tau_2^0) = -17.11 \pm 2.62).$$

As the large error values show, the results are not very reliable. In addition, T_{VF} is a bit too low for investigating the connected low-temperature process more precisely with the DMA apparatus. Nevertheless, the results seem to indicate that the temperature dependence of τ_2^{rel} is described better by a Vogel–Fulcher law than by an Arrhenius law.

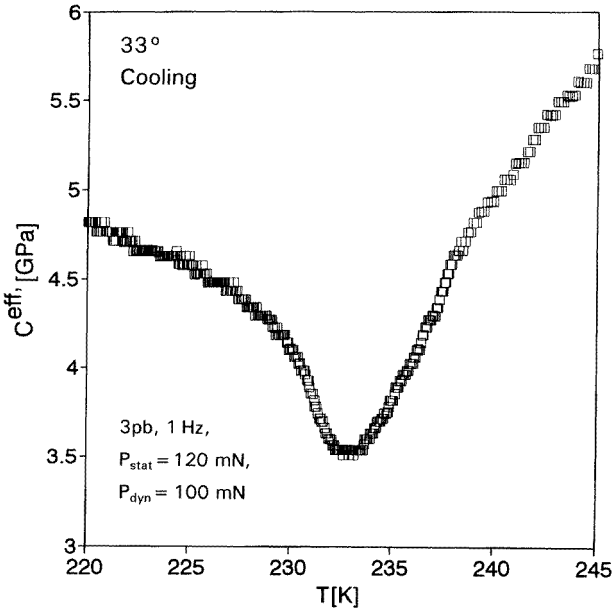

Figure 6. Measured values of $C^{eff\,\prime}$ for a sample with L oriented along $\theta_1 = 33^\circ$.

2.3.3. Direction dependence. In connection with the hypothesis of ferroelastic domain freezing (compare sections 3.2.1 and 4.1), three-point-bending measurements have been performed on samples whose edges were parallel and perpendicular to the direction of the domain walls (33° with respect to the crystallographic a-axis), because no influence of domain wall motion on the elastic constant is expected in this direction. Therefore the temperature dependence of the elastic constant should display the behaviour of a monodomain crystal. These measurements proved to be difficult because many samples broke at T_c or in the region below T_c. This might have been due to the high stiffness of ALHS if stressed along this direction [9]. The resulting $C^{eff\,\prime}$ (33°) is shown in figure 6. For decreasing temperature $C^{eff\,\prime}$ decreases, too, reaching a minimum at around T_c. Then $C^{eff\,\prime}$ increases again, as expected for a crystal where there is no contribution of moving domain walls to the elastic constant (see also the discussion in section 4.1).

3. Fundamental theoretical considerations

Before interpreting the experimental results, a theoretical basis on which to explain the observed domain wall effects in ALHS has to be developed. Mainly, three questions are connected to this.

(1) Under which circumstances (applied external fields etc) does domain wall motion occur in ALHS?

(2) Is it possible to stimulate domain wall motion with a given experimental method or not? The answer to this can help one to distinguish domain wall effects from others.

(3) How does the motion of domain walls affect the (low-frequency) elastic properties of a crystal?

The answers to these questions will be given in the following sections where three different methods of low-frequency elastic measurement will be considered.

3.1. Domain switching in ALHS

A domain wall between two ferroelastic orientation states S_1, S_2 starts to move when the energetical equilibrium between S_1 and S_2 is disturbed (the difference between their Gibbs free-energy densities $\Delta\Phi \neq 0$). In this case the state with the lower energy density enlarges at the cost of the other orientation state.

Therefore one has to find the dependence of this energy difference on external influences for a crystal belonging to the Aizu species 4F2 (No 78) [20].

The difference between the Gibbs free-energy densities of two orientation states of a pure ferroelastic crystal which is exposed only to the stress components σ_{ij} is given by (see p 18 of [21])

$$\Delta\Phi = \Phi(S_2) - \Phi(S_1) = -\Delta e^s_{ij}\,\sigma_{ij} - \frac{1}{2}\Delta S_{ijkl}\,\sigma_{ij}\sigma_{kl} - \cdots \tag{6}$$

where the last term denotes the ferrobielastic contribution (see p 19 of [21]).

For the Aizu species 4F2, $\Delta\Phi$ [9] is

$$\begin{aligned}\Delta\Phi = {} & 2e(\sigma_1 - \sigma_2 + q\sigma_6) - \frac{1}{2}[(S_{22} - S_{11})(\sigma_1^2 - \sigma_2^2) + 2(S_{23} - S_{13})(\sigma_1\sigma_3 - \sigma_2\sigma_3) \\ & - 2(S_{16} + S_{26})(\sigma_1\sigma_6 + \sigma_2\sigma_6) \\ & - 4S_{36}\sigma_3\sigma_6 + (S_{55} - S_{44})(\sigma_4^2 - \sigma_5^2) - 4S_{45}\sigma_4\sigma_5]\end{aligned} \tag{7}$$

where $e = e^s_{11}$ is a component of the tensor of spontaneous strain, which is related to the component $f = e^s_{12}$ by $q = 2f/e$. If the external uniaxial stress σ is applied in a general direction, the stress components are given by (see p 68 of [21])

$$\sigma_{ij} = l_i l_j \sigma \qquad l_i = \cos\theta_i. \tag{8}$$

The θ_i are the angles between the general direction and the axis x_i, and the following identity is valid:

$$l_1^2 + l_2^2 + l_3^2 = 1. \tag{9}$$

Inserting equation (8) in (7) one gets the dependence of the difference of the Gibbs free-energy densities $\Delta\Phi$ on the applied stress σ and the direction cosines:

$$\begin{aligned}\Delta\Phi = {} & 2e\sigma(l_1^2 - l_2^2 + q l_1 l_2) - \frac{\sigma^2}{2}[(S_{22} - S_{11})(l_1^4 - l_2^4) - 2(S_{16} + S_{26})(l_1^3 l_2 + l_2^3 l_1) \\ & + (2S_{23} - 2S_{13} + S_{44} - S_{55})(l_1^2 l_3^2 - l_2^2 l_3^2) - 4(S_{36} + S_{45})l_3^2 l_1 l_2].\end{aligned} \tag{10}$$

3.2. Stimulation of domain wall motion by various experimental methods

3.2.1. Stimulation by three-point bending. A detailed analysis [9] showed that for three-point bending

$$\Delta\Phi = \sigma_l\left\{2e(Q + qR) + \frac{\sigma_l}{2}[(S_{11} - S_{22})Q + 2(S_{16} + S_{26})R]\right\}$$
$$= \sigma_l\{U(\cos^2\theta_1 - \sin^2\theta_1) + 2V\cos\theta_1\sin\theta_1\} \tag{11}$$

where $Q = \cos^2\theta_1 - \sin^2\theta_1$, $R = \cos\theta_1\sin\theta_1$, $U = 2e + (\sigma_l/2)(S_{11} - S_{22})$, and $2V = 2eq + \sigma_l(S_{16} + S_{26})$. Hence, generally speaking, the domain walls will be moving within a c-plate of ALHS which is subject to three-point bending.

Setting equation (11) equal to zero one finds that in full agreement with physical considerations which lead one to expect four equivalent directions in a crystal with two orientations of domain walls perpendicular to each other, there are four directions θ_1 where no domain wall motion can be excited (φ is the angle between the domain wall and the tetragonal a-axis):

$$\theta_1 = \left\{\varphi,\ \varphi + \frac{\pi}{2},\ \varphi + \pi,\ \varphi + \frac{3\pi}{2}\right\}. \tag{12}$$

The motion of the domain wall within the sample due to external stress leads to an additional contribution, which is why the entire strain e^{eff} is thus composed of the pure elastic contribution e^{elast} and a contribution e^{DW} due to domain wall motion [9]:

$$e^{eff} = e^{elast} + e^{DW}. \tag{13}$$

The resulting elastic compliance S^{eff} is then given by

$$S^{eff} \approx \frac{4H^3D}{PL^3}(u^{elast} + u^{DW}). \tag{14}$$

3.2.2. Stimulation by the parallel-plate technique. Geometrically, the parallel-plate method may be treated as a simpler special case of the three-point-bending method. All of the parallel-plate results presented in this work have been obtained for configurations where the uniaxial stress was applied along one of the crystallographic axes. Therefore the considerations may be restricted to three cases: $\boldsymbol{\sigma} \parallel a$, $\boldsymbol{\sigma} \parallel b$, and $\boldsymbol{\sigma} \parallel c$. Because for each of these configurations only one stress component $\sigma_i \neq 0$, Hooke's law reduces to

$$e_i = S_{ii}\sigma_i. \tag{15}$$

According to equation (7), $\Delta\Phi = 0$ if only σ_3 is applied. *In such a case one would not expect a change of the elastic compliance due to moving domain walls.* The experimental results are in accordance with this.

For the other two directions of σ, $\Delta\Phi$ is given by (following from equation (7))

$$\Delta\Phi = 2e(\sigma_1 - \sigma_2) + \frac{S_{11} - S_{22}}{2}(\sigma_1^2 - \sigma_2^2). \tag{16}$$

Like for three-point-bending measurements the elastic compliance is a sum of two contributions [9]:

$$S^{eff} = S^{elast} + S^{DW}. \tag{17}$$

Because e^{DW} has the same sign as the applied stress, $S^{DW} > 0$, thus leading to a softer crystal behaviour than expected from pure elastic calculations.

3.2.3. Stimulation with a torsion pendulum. Although no results obtained with the torsion pendulum technique are presented in this work, it will prove to be of significance for dealing with this kind of experiment. As there are almost no low-frequency elastic results available for ALHS, everything which has been published until now has to be referred to measurements presented by Mróz *et al* performed with a torsion pendulum [4]. Their results will be used for estimations concerning the relaxation processes of domain walls in ALHS. Studying the applied method [22], one finds that the resonance frequencies were in the region of 200 Hz, which is higher by a factor of four than the highest frequencies within reach of the DMA apparatus.

A detailed analysis of three different geometrical situations [9] shows that if the torsion axis is parallel to the z-axis there should be domain wall motion induced only by higher (ferrobielastic) coupling.

The situation is different if the torsion axis coincides with the x- or the y-axis of the coordinate system. Then domain wall motion is expected due to ferroelastic coupling. Only the application of a stress component σ_6 may cause a ferroelastic shifting of the domain walls (which is equivalent to the fact that the torsion axis is parallel to the x- or the y-axis).

As a consequence the influence of domain wall motion should hence be observed also with a torsional pendulum—provided that the resonance frequencies of the sample are within the frequency range where domain wall shifting can be induced.

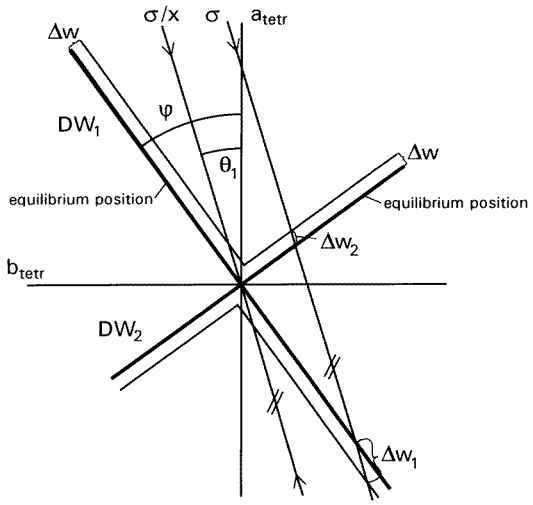

Figure 7. Geometrical relationships for domain wall shifting.

3.3. Estimation of domain wall motion parameters

As has been discussed already, the observed elastic behaviour between T_c and T_f can be accounted for by moving domain walls producing an additional contribution to the elastic compliance of ALHS. Until now no quantitative description of this domain wall motion has been given. In this section it is our aim to estimate some basic quantities related to the domain structure. As has been stated before, the reason for the motion of the domain walls lies in a difference $\Delta\Phi$ between the potentials of the two orientation states S_1 and S_2. This difference is induced by external stress. In the case of a friction-free domain wall motion

one would expect a vanishing coercive stress for ferroelastic domain switching; i.e., even for a very small stress (or $\Delta\Phi$) all of the domain walls would cross the crystal boundaries thus leaving a monodomain sample. Because this has not been observed it is legitimate to assume a relationship between $\Delta\Phi$ and the resulting domain wall shift Δw. Hence the following Taylor series expansion will be used:

$$\Delta w(\Delta\Phi) = \Delta w(0) + \left.\frac{\partial w}{\partial \Delta\Phi}\right|_0 \Delta\Phi + \left.\frac{\partial^2 w}{\partial \Delta\Phi^2}\right|_0 \Delta\Phi^2. \tag{18}$$

Taking into account the first two terms, the expansion reduces to a linear function of $\Delta\Phi$ because $\Delta w(0) = 0$. Again, the applied stress is restricted to the x–y-plane and ferrobielastic contributions are neglected. Thus equation (18) transforms after insertion of equation (10) to

$$\Delta w = C_{\phi w}\,\Delta\Phi = 2C_{\phi w} e\sigma(\cos^2(\theta_1) - \sin^2(\theta_1) + q\cos(\theta_1)\sin(\theta_1)) \tag{19}$$

where $C_{\phi w}$ is a measure for the domain wall mobility. Equation (19) can be transformed [9] to

$$\Delta w(\theta_1, \varphi) = \frac{2C_{\phi w} e\sigma \sin 2(\varphi - \theta_1)}{\sin 2\varphi} \tag{20}$$

where θ_1 again denotes the angle between the direction of the applied stress and the crystallographic a-direction, and φ denotes the angle between the a-axis and the domain wall (see figure 7). Besides this, it stands to reason that the solutions found in equation (12) for the condition of zero domain wall motion fulfil also equation (20).

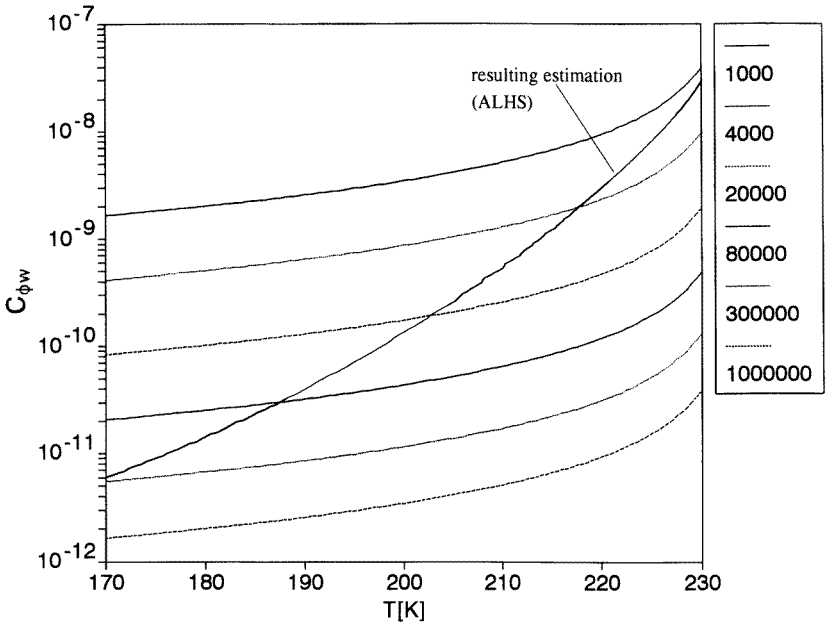

Figure 8. Calculated temperature dependences of the coefficient $C_{\phi w}$ for several values of the domain wall density ρ^{DW} (m^{-1}).

The calculation of $C_{\phi w}$ can be found in the appendix and yields

$$C_{\phi w}(T) = \frac{2F_1 + X(T)}{Y(T)\rho^{DW}(T)a^t(T)}.$$

According to this $C_{\phi w}$ was calculated for the temperature interval between 170 K and 230 K, i.e., for the interval where S^{eff} is only weakly temperature dependent. The reason for that is that below this temperature region, S^{eff} starts to decrease at around T_f, and the domain walls cannot move freely any more. Not far above 230 K the domain pattern vanishes because of the phase transition to the tetragonal high-temperature phase. The experimental values obtained for the region of 170 K–230 K are approximated by a linear temperature behaviour, where C^{eff} (170 K) is set equal to 6×10^8 Pa and C^{eff} (230 K) is set equal to 4×10^8 Pa. It is obvious that $0 < F_1 < 1$. As calculated, $X(T)$ varies between $\approx$80 and 50 for the temperature interval 170 K–230 K. Therefore the contribution of F_1 may be neglected. With the help of equation (A11) this allows the calculation of the temperature dependence of $C_{\phi w}$ for given temperature-independent values of ρ^{DW}. This has been done for values of ρ^{DW} between 10^3 m^{-1} and 10^6 m^{-1} (for F_1 the value 0.5 was inserted)—the results are shown in figure 8. As can be seen, $C_{\phi w}$ decreases with lowering temperature and thus *the domain wall mobility decreases*. Resulting consequences will be reported and dealt with in future work.

The typical (temperature-dependent) values of domain wall densities are within the above-mentioned region for ALZX crystals (Z = H, D; X = S, Se); therefore at least the order of magnitude of $C_{\phi w}(T)$ may be estimated. In ALHS, ALHSe and in ALDSe, ρ^{DW} increases with decreasing temperature. The value of ρ^{DW} in ALHSe lies between 10^3 and 10^4 approximately 15 K below T_c and in the region of 10^5 about 45 K below T_c [2]. For ALDSe $\rho^{DW} \cong 3 \times 10^5$ at 60 K below T_c [23]. Using these values for the estimation for ALHS, one finds from figure 8 that $C_{\phi w}(T)$ decreases by about three orders of magnitude between 230 K and 170 K. Hence for $\theta_1 = 0$ the resulting domain wall shift is approximately given by (see equation (20))

$$\Delta w(\approx 170\ \text{K}) \approx \sigma \times 10^{-13}\ \text{m}$$
$$\Delta w(\approx 230\ \text{K}) \approx \sigma \times 10^{-10}\ \text{m}.$$

This yields a *variation of Δw between $\approx$100 Å and $\approx$10 μm* (thus the domain walls are expected to be easily movable in the region near T_c). It is interesting to compare these values with that of the amplitude of lateral displacement of domains in, e.g., ferroelectric KH_2PO_4 (KDP) which was found to be of the order of 10 Å. In addition, the domain wall thickness was estimated to be about 500 Å (a hundred times the lattice spacing) in KDP [24]. In Rochelle salt the thickness of the ferroelectric domain walls was determined to be between 500 Å and 2500 Å [25]. Also values of 30–70 Å and 12–220 Å have been reported for KDP and Rochelle salt, respectively [26].

4. Further considerations

In the following, some of the main features found in the temperature dependence of C^{eff} and described in section 2.3 will be discussed and as far as possible explained.

4.1. Ferroelastic domain freezing

The most striking result is that of $C_{11}^{eff\prime}$ remaining almost constant over a broad temperature region below T_c, while one would expect a steep rise starting right at T_c. Around T_f, $C_{11}^{eff\prime}$

exhibits a rise which is accompanied by a maximum of $C_{11}^{eff\,\prime\prime}$.

Up to this point of the work, domain wall motion has been discussed only for the case of a static external stress σ being applied to the sample. Now a thermally activated domain wall relaxation process with a relaxation time τ_1^{rel} will be considered (compare also the discussion of the domain wall mobility in section 3.3). Hence for a Debye relaxation (compare, e.g., p 94 in [27]) one would expect the following for the frequency-dependent elastic constant $C(\omega_{appl}, \tau_1^{rel})$ if a driving force (i.e., external stress) is applied with a given frequency ω_{appl}:

$$C'(\omega_{appl}, \tau_1^{rel}) = C(\omega = \infty) - \frac{C(\omega = \infty) - C(\omega = 0)}{1 + \omega_{appl}^2\ (\tau_1^{rel})^2} \tag{21a}$$

$$C''(\omega_{appl}, \tau_1^{rel}) = \frac{C(\omega = \infty) - C(\omega = 0)}{1 + \omega_{appl}^2 (\tau_1^{rel})^2} \omega_{appl} \tau_1^{rel}. \tag{21b}$$

Assuming now τ_1^{rel} to rise with decreasing temperature, while keeping ω_{appl} constant, the following is expected.

Equations (21*a*) and (21*b*) imply a rise of $C'(\omega_{appl} = \text{constant}, \tau_1^{rel})$ and a maximum of $C''(\omega_{appl} = \text{constant}, \tau_1^{rel})$ at around T_f—where T_f is equivalent to the temperature for which $\omega_{appl}\tau_1^{rel} \approx 1$. Above T_f, $\omega_{appl}\tau_1^{rel} < 1$, i.e. the applied frequency is low enough for the domain walls to follow the external stimulation. *Below T_f, $\omega_{appl}\tau_1^{rel}$ becomes >1; the relaxation time τ_1^{rel} is now too large for the external dynamic stress to stimulate the domain wall motion with which τ_1^{rel} is associated ('domain freezing').*

In general, T_f is expected to increase with rising ω_{appl}. However, no clear frequency dependence of T_f could be found in DMA experiments. Hence it is concluded that T_f is quite near a static limit for frequencies $\leqslant$50 Hz. As a consequence—and in accordance with the ferroelectric case of KDP [18]—a Vogel–Fulcher law is assumed to be valid:

$$\tau_1^{rel} = \tau_1^0 \exp\left(\frac{E_1^{act}}{T - T_{VF}}\right). \tag{22}$$

Because the narrow frequency interval accessible with the DMA apparatus did not allow us to observe a clear frequency dependence of T_f, only the simplest case will be considered here. Thus the activation energy was assumed to be a single temperature-independent value E_1^{act} (compare again [18] where a temperature-independent distribution of E_1^{act} is assumed). An additional reason for the difficulties in determining the frequency dependence of T_f might be that already given by Kuramoto who observed a dependence of T_{VF} on the specimens and on the run of the measurement.

In addition, results for higher frequencies have to be taken into account. Until now, only results obtained by Brillouin scattering and by the torsion pendulum technique have been published for ALHS. The resonance frequencies of the torsion pendulum measurements lie in the region of 200 Hz. According to section 3.2.3 *moving domain walls produce a lowering of the measured torsion modulus*. As can be seen from [4] *no such lowering has been observed*.

Thus it is clear that $T_f \geqslant T_c$ for $\omega_{appl} \approx 200$ Hz. Although the lack of a clear determination of T_f for this frequency proves a disadvantage, at least an estimation of the parameters of the Vogel–Fulcher dependence may be achieved. Each value obtained for T_f by DMA experiments is known only within an error interval of ± 0.5 K. Thus it is conceivable that there is a slight frequency dependence of T_f which is 'hidden' within the resulting uncertainty of ± 5 K. In fact it is a consequence of the assumed Vogel–Fulcher dependence that T_f(1 Hz) lies at least slightly below T_f(50 Hz). For the following estimation it was presumed that the difference between T_f(1 Hz) and T_f(50 Hz) is equal to the error

interval. Together with the result $T_f(200\ \text{Hz}) \geqslant T_c$, this makes it possible to determine an upper limit for E_1^{act}: in the event of the above assumption being incorrect it is clear that $T_f(1\ \text{Hz})$ and $T_f(50\ \text{Hz})$ can lie only nearer together than estimated. $T_f(200\ \text{Hz})$ may be higher than T_c. Both cases would lead to a stronger curvature of the resulting Vogel–Fulcher curve, thus producing lower values of E_1^{act}. Calculating a Vogel–Fulcher curve going through the points (157 K, 1 Hz), (167 K, 50 Hz), and (T_c, 200 Hz) one obtains

$$E_1^{act} \cong 0.002\ \text{eV}\ (24\ \text{K}) \qquad T_{VF} \cong 152.5\ \text{K} \qquad \tau_1^0 \cong 6 \times 10^{-4}\ \text{s}.$$

Calculating the parameters for (162 K, 1 Hz), (162.2 K, 50 Hz), and (250, 200 Hz) one obtains

$$E_1^{act} \cong 3.3 \times 10^{-5}\ \text{eV}\ (0.38\ \text{K}) \qquad T_{VF} \cong 161.9\ \text{K} \qquad \tau_1^0 \cong 7.9 \times 10^{-4}\ \text{s}.$$

In addition, a very rough estimation of the temperature dependence of τ_1^{rel} can be given. As $\tau_1^{rel} \approx 1/\omega_{appl}$ at T_f one gets

$$3 \times 10^{-3}\ \text{s} \leqslant \tau_1^{rel} \leqslant 0.15\ \text{s} \qquad \text{for} \cong 162\ \text{K}$$
$$7.5 \times 10^{-4}\ \text{s} \leqslant \tau_1^{rel}\ \text{s} \qquad \text{for}\ T_c.$$

As discussed in section 3.2.1, *no domain wall motion is expected if the external stress is applied parallel and perpendicular to the domain wall orientations. The corresponding experimental result is shown in figure 6:* below T_c, $C^{eff\prime}$ rises again indicating that there is (almost) no domain wall contribution to the elastic compliance (compare equation (17)). The inhomogeneous stress profile induced by three-point bending (compare section 2.2) leads to a 'smearing out' of the phase transition which can be seen in figure 6.

4.2. Additional features and open questions

Beyond the 'domain freezing' described in the preceding section, two additional phenomena have been observed which seem to be closely connected to the domain (wall) properties of ALHS: a 'history' dependence and residual domain wall motion below T_f.

If a sample is exposed to temperature cycling $C_{11}^{eff\prime}$ *rises during the later runs to much higher values below* T_f *than during the first run* (i.e., the first cooling and heating; figure 1). Also, the low-temperature damping maximum decreases and vanishes for later runs (figure 4). There may be a certain connection between the two features. It is also interesting that the low-temperature damping reaches much higher values for samples used in experiment for the very first time (figure 2). The highest values of $C_{11}^{eff\prime}$ below T_f are of about the same magnitude as those at room temperature, i.e., the crystal is nearer to a monodomain state. This and the magnitude of the activation energy of the process which leads to the low-temperature damping maximum (section 2.3.2) suggest that *some kind of domain wall relaxation is also involved below* T_f. However, the process must be different from that observed above T_f, as the low-temperature damping and some remaining damping around T_f are observed even for stress values in the region of MPa [9]. One possibility might be that *even below* T_f *at least a part of the domain walls performs small oscillations around pinned positions (instead of shifts), in contrast to the case for the temperature region above* T_f *where shifting of the domain walls is also possible. Hence the 'domain freezing' is not a total one.* The above would also explain why the ratio of the values of $C_{11}^{eff\prime}$ below and above T_f shows a dependence on static stress [9]: if static stress is applied, domain walls are shifted above T_f, while this does not occur below T_f.

The following consideration might account for the 'history' dependence: within a sample having crossed the phase transition temperature only once before (a 'virgin sample'), $C_{11}^{eff\prime}$

clearly does not reach (above and below T_f) the value expected for a crystal whose domain walls are more or less immovable. So at least a part of the domain walls oscillates also below T_f, thus producing the low-temperature damping maximum (see above). After heating above T_c and cooling back again continuously, we assume that internal stress ('transition debris' etc) begins to hinder the domain wall motion. Therefore even above T_f, the values of $C_{11}^{eff\prime}$ are higher than for a fresh crystal. In particular the type of domain wall relaxation still existing below T_f is suppressed by internal stress and so $C_{11}^{eff\prime}$ increases below T_f more than within a virgin sample.

The hypothesis of internal stress influencing the elastic behaviour of ALHS crystals is corroborated by the fact that a sample cooled down below T_c several times and afterwards *heated up to a temperature of ∼400 K or more shows again the behaviour of a virgin crystal* (compare [10] where something similar is reported for ALHS, too). *Annealing takes place also at room temperature if the crystal is kept at zero external stress for several hours.* Thus one may say that virgin samples are in a kind of 'ground state', which is left after the first cooling and heating cycle. The crystal returns to this ground state by itself if the value of the 'product of provided temperature and time' is large enough. Hence for low temperatures one would expect very long annealing times (under the assumption that annealing actually can take place at low temperatures). Indeed, keeping a virgin sample as well as a crystal exposed to the second run of temperature cycling at a temperature of ≈100 K at zero external stress for 8 h did not change the actual elastic behaviour of the sample, which is in accordance with the expectations.

In addition, there might be also a connection between the annealing behaviour of the crystal and the hindrance of macroscopic domain wall motions: on the one hand one expects much higher annealing times for lower temperatures, and on the other hand domain walls are more hindered in their motion at lower temperatures. This leads to the conclusion that internal stress concentrations are reduced via temperature-activated motions to which domain wall motion is related (compare also figure 8).

5. Conclusions

It has been shown in this work that the low-frequency elastic anomalies observed in the ferroelastic phase of ALHS result from the motion of domain walls (compare also optical domain studies which give a clear hint of the dynamic character of the phenomena [9]). The elastic behaviour in the temperature region between T_c and T_f can be explained by (vibrational and lateral) domain wall motions reaching amplitudes of some μm directly below T_c. These amplitudes decrease with decreasing temperature due to an increase of the related relaxation time τ_1^{rel}. Simultaneously, the macroscopic mobility of the domain walls decreases and the coercive stress rises due to the increased energy difference between the two possible ferroelastic orientation states. Around $T_f \cong 162$ K a distinct lowering of domain wall mobility occurs *(partial 'domain freezing')* leading to an increase of the storage modulus and to a maximum of the loss modulus. To the knowledge of the authors, this is the first time that pure ferroelastic domain freezing has been reported. In ALHS, 'domain freezing' seems to be a 'freezing' of motional degrees of freedom of the domain walls. This freezing is 'anticipated' by the decreasing domain wall mobility with lowering temperature.

For the frequency range accessible with the DMA apparatus, T_f has almost reached its static limit and therefore no frequency dependence of T_f could be observed. A rough

estimation, assuming a Vogel–Fulcher dependence of τ_1^{rel}, yields

$$E_1^{act} \leqslant 0.002 \text{ eV} \qquad 152 \text{ K} \leqslant T_{VF} \leqslant 162 \text{ K} \qquad 6 \times 10^{-4} \text{ s} \leqslant \tau_1^0 \leqslant 8 \times 10^{-4} \text{ s}.$$

Below T_f the domain walls seem to retain a certain (vibrational) mobility, which is expressed in the fact that the storage modulus remains rather small while the loss modulus exhibits an additional maximum at low temperatures. The parameters of this relaxation process obtained by a fit with a Vogel–Fulcher law are

$$E_2^{act} \cong 0.0036 \pm 0.0040 \text{ eV} \qquad T_{VF} \cong 85.5 \pm 8.3 \text{ K} \qquad \tau_2^0 \cong 1.7 \times 10^{-3} \text{ s}.$$

During later runs of temperature cycling an increase of the measured storage modulus $C^{eff\,\prime}$ has been found. It seems that if a crystal is exposed to more than one consecutive run of cooling and heating then, as well as the domain wall motion between T_c and T_f, the low-temperature relaxation ($T < T_f$) is in particular affected by remaining internal stresses. As we have observed in our experiments, *these internal stresses can be removed either by heating the sample above room temperature or by allowing enough time at room temperature without loading*.

Due to the fact that the frequency range of the DMA was too small for us to obtain clear data on the frequency dependence of T_f, we suggest carrying out additional investigations in the frequency interval between 50–200 Hz. Future adaptations of the DMA apparatus will most probably allow measurements of the low-temperature relaxation below 100 K also. The behaviour of ALHS crystals exposed to high uniaxial stress during cooling will be interesting to study in future, too.

Acknowledgments

The authors are grateful to A Fuith for advice on growing the crystals. Thanks are also due to J Rosenstingl for performing the powder diffraction records.

This work was supported by the Österreichischer Fonds zur Förderung der wissenschaftlichen Forschung under project number P9793-PHY.

Appendix. Calculation of the parameter $C_{\phi w}$

As the domain walls in ALHS are perpendicular with respect to each other, there are four possible values of the domain wall angle φ. Because of the form of $\Delta w(\theta_1, \varphi)$ it is sufficient to check the angular dependence of Δw for a second domain wall (DW_2) perpendicular to the first one (DW_1). Insertion of $\varphi - 90^\circ$ instead of φ yields again equation (20). Thus it is obvious that the system of domain wall orientations is sufficiently described if just φ is taken into account.

During parallel-plate measurements the external stress is applied in the same direction as where the displacement is measured. It is therefore of great interest to calculate the change of this displacement due to domain wall shifts within the sample. The simplest way of expanding an orientation state (domain) is given by domain walls whose directions of shift are perpendicular to the domain walls themselves. Therefore an additional geometrical consideration has to be carried out in order to find Δw in relation to the change of the crystal length along the direction of applied stress: generally for a given direction of applied stress θ_1, the projections of Δw will be different for DW_1 (Δw_1) and for DW_2 (Δw_2). They are given by

$$\Delta w_1 = \frac{\Delta w}{\sin(\varphi - \theta_1)} \qquad \text{and} \qquad \Delta w_2 = \frac{\Delta w}{\cos(\varphi - \theta_1)}. \tag{A1}$$

The contribution in the direction of θ_1 produced by the shift of two single-domain walls perpendicular to each other is given by

$$\Delta w^{pair} = \Delta w_1 + \Delta w_2. \tag{A2}$$

It is sufficient to take into account only those values of θ_1 for which $\Delta w \neq 0$. Besides this, it is necessary to distinguish between $\theta_1 > \varphi$ and $\theta_1 < \varphi$. As $\theta_1 + 180^\circ$ is equivalent to θ the remaining cases are as follows.

(1) $\varphi > \theta_1 > \varphi - 90^\circ$:

$$\Delta w^{pair}(\varphi > \theta_1 > \varphi - 90^\circ) = \frac{4C_{\phi w} e\sigma(\sin(\varphi - \theta_1) + \cos(\varphi - \theta_1))}{\sin 2\varphi}. \tag{A3}$$

(2) $\varphi + 90^\circ > \theta_1 > \varphi$:

$$\Delta w^{pair}(\varphi + 90^\circ > \theta_1 > \varphi) = \frac{4C_{\phi w} e\sigma(\sin(\varphi - \theta_1) - \cos(\varphi - \theta_1))}{\sin 2\varphi}. \tag{A4}$$

The majority of the measurements have been performed for stress applied along the crystallographic a-direction. Therefore the following calculations will be reduced to the case where $\theta_1 = 0$. Neglecting the shear component of the order parameter, the change of length along the a-direction induced by two shifting domain walls is given by $2e\,\Delta w^{pair}$. Hence the total change of length is

$$\Delta w^{\Sigma} = e\,\Delta w^{pair}\, n^{DW} \tag{A5}$$

where n^{DW} denotes the number of domain walls intersecting a line parallel to the (tetragonal) a-axis (compare figure 7). Here it is assumed that n^{DW} is constant (with some tolerance) for all possible lines parallel to the a-axis. In addition, it is presumed that n^{DW} is an even number. Both assumptions are not very restrictive for domain wall densities, as observed (see section 3.3).

In the following a simple model is constructed in order to calculate the relationship between domain structure and the physical extent of a crystal: n^{uc} is the total number of unit cells along the a-direction, of which s_1 are in the orientation state S_1 and $n^{uc} - s_1$ are in the orientation state S_2 for zero external stress (here the regions within domain walls are neglected). The average length of the crystal is $n^{uc}a^t(T)$, where $a^t(T)$ is the extrapolated tetragonal lattice parameter $a^t(T) = a(RT)(1 - \alpha_{ex}(RT - T))$. The ferroelastic distortion in S_1 produces an additional contribution $e(T)s_1a^t(T)$; S_2 produces $-e(T)(n^{uc} - s_1)a^t(T)$. Thus the resulting crystal length l_0 parallel to the a-direction is, at the temperature T,

$$l_0(T) = a^t(T)(2e(T)s_1 + n^{uc}(1 - e(T))). \tag{A6}$$

The strain induced by domain wall shifts is then calculated from

$$e_1^{DW} = \frac{\Delta w^{\Sigma}}{l_0}. \tag{A7}$$

Combining equations (A5), (A6), (15), (13), and (17) one obtains

$$a^t(T)\sigma_1(S_{11}^{eff}(T) - S_{11}^{elast}(T)) = \frac{\Delta w^{pair}(T) n^{DW}}{2s_1 + n^{uc}(1/e(T) - 1)} \tag{A8}$$

which is transformed with the aid of equation (A3) to

$$\frac{4e(T)(\sin\varphi + \cos\varphi)}{(S_{11}^{eff}(T) - S_{11}^{elast}(T))a(RT)(1 - \alpha_{ex}(RT - T))\sin 2\varphi}$$
$$= \frac{2F_1}{C_{\phi w}\rho_{uc}^{DW}} + \frac{1}{C_{\phi w}\rho_{uc}^{DW}}\left(\frac{1}{e(T)} - 1\right) = Y(T) = \frac{2F_1}{C_{\phi w}\rho_{uc}^{DW}} + \frac{1}{C_{\phi w}\rho_{uc}^{DW}} X(T) \tag{A9}$$

where $F_1 = s_1/n^{uc}$ is the portion of unit cells in the orientation state S_1 and $\rho_{uc}^{DW} = n^{DW}/n^{uc}$ the number of domain walls per side length of a unit cell. $X(T)$ and $Y(T)$ consist only of quantities known from calculations [9] or experiments (see sections 1, 2.3.1) and can therefore be determined.

Also F_1, $C_{\phi w}$, and ρ_{uc}^{DW} can be temperature dependent. A temperature dependence of the domain pattern is indeed reported in [10] for ALHS, in [28] for ALDS, in [2] for ALHSe, and in [23] for ALDSe crystals. Mostly domain wall densities are estimated by observation through a polarizing microscope and are given in m^{-1}. Thus ρ_{uc}^{DW} is transformed into the number of domain walls per metre by

$$\rho^{DW}(T) \cong \frac{\rho_{uc}^{DW}(T)}{a^t(T)}. \tag{A10}$$

Now it is of great interest to estimate the magnitude of the coefficient $C_{\phi w}$ which relates $\Delta\Phi$ to the resulting domain wall shift Δw.

Transforming equation (A9) and inserting (A10) yields

$$C_{\phi w}(T) = \frac{2F_1 + X(T)}{Y(T)\rho^{DW}(T)a^t(T)}. \tag{A11}$$

References

[1] Pietraszko A, Połomska M and Pawłowski A 1991 *Bull. Acad. Sci. USSR Phys. Ser.* **55** 109–11
[2] Połomska M, Pawłowski A, Smutný F and Wolak J 1993 *Ferroelectrics* **140** 299–304
[3] Knite M, Schranz W, Fuith A and Warhanek H 1993 *J. Phys.: Condens. Matter* **5** 9099–104
[4] Mróz B, Piskunowicz P, Pawłowski A and Krajewski T 1994 *Ferroelectrics* **159** 155–9
[5] Mróz B, Kiefte H, Clouter M J and Tuszyński J A 1993 *J. Phys.: Condens. Matter* **5** 6377–86
[6] Mielcarek S, Tylczyński Z and Mróz B 1995 *EMF-8 (Nijmegen, 1995)* abstracts, p P06:55
[7] Pawłowski A 1994 *4th Int. Symp. on Systems with Fast Ionic Transport (Warszawa-Miedzeszyn, Poland,1994)*
[8] Zimmermann M and Schranz W 1994 *Acta Phys. Slovaca* **44** 429–33
[9] Zimmermann M 1995 *PhD Thesis* University of Vienna (in English)
[10] Mielcarek S, Tylczyński Z, Piskunowicz P and Mróz B 1995 *Ferroelectrics* **172** 287–94
[11] Zimmermann M, Schranz W, Warhanek H, Apih T, Lahajnar G, Blinc R and Pawłowski A 1995 *Solid State Commun.* **95** 749–52
[12] Blinc R, Lahajnar G, Seliger J, Zupančič I, Zimmermann M, Fuith A, Schranz W and Warhanek H 1994 *Solid State Commun.* **92** 765–7
[13] Zimmermann M, Schranz W, Blinc R, Lahajnar G and Apih T 1994 *3rd Int. Symp. on Domain Structure of Ferroelectrics and Related Materials—ISFD-3 (Zakopane, Poland, 1994)*
[14] Fally M, Kubinec P, Fuith A, Warhanek H and Filipič C 1995 *J. Phys.: Condens. Matter* **7** 2195–204
[15] Rinnerthaler S 1994 *Master's Thesis* University of Vienna (in German)
[16] Rossiter B W and Baetzold R G (ed) 1991 *Determination of Elastic and Mechanical Properties (Physical Methods of Chemistry VII)* 2nd edn (New York: Wiley)
[17] Voigt W 1910 *Lehrbuch der Kristallphysik (Teubners Sammlung von Lehrbüchern auf dem Gebiete der Mathematischen Wissenschaften XXXIV)* (Leipzig: Teubner)
[18] Kuramoto K 1987 *J. Phys. Soc. Japan* **56** 1859–67
[19] Jäckle J 1986 *Rep. Prog. Phys.* **49** 171–231
[20] Aizu K 1970 *Phys. Rev.* B **2** 754–72
[21] Wadhawan V K 1982 *Phase Transitions* **3** 3–103
[22] Gridnev S A, Postnikov V S, Prasolov B N, Shuvalov L A and Fedosyuk R M 1978 *Ferroelectrics* **21** 597–9
[23] Połomska M and Pawłowski A 1994 *Ferroelectrics* **157** 93
[24] Bornarel J and Lajzerowicz J 1968 *J. Appl. Phys.* **39** 4339–41
[25] Gurk P 1972 *Phys. Status Solidi* a **10** 407–14
[26] Schranz W 1995 *Key Eng. Mater.* **101+102** 41–60
[27] Debye P 1929 *Polar Molecules* (New York: Dover)
[28] Połomska M and Pawłowski A 1995 *Ferroelectrics* **172** 315–8